Article

Fourier Transform Infrared Characterization of a Cu–Nitrosyl Complex in Cytochrome *ba* from *Thermus thermophilus*: Relevance to NO Reductase Activity in Heme–Copper Terminal Oxidases

Takahiro Hayashi, I-Jin Lin, Ying Chen, James A. Fee, and Pierre Monne-Loccoz

J. Am. Chem. Soc., **2007**, 129 (48), 14952-14958 • DOI: 10.1021/ja074600a

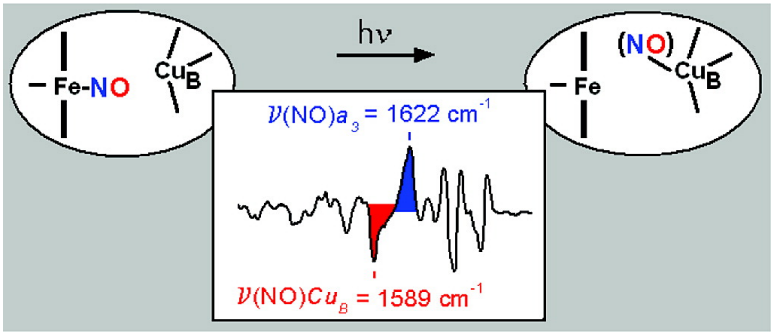

More About This Article

Additional resources and features associated with this article are available within the HTML version:

- Supporting Information
- Links to the 1 articles that cite this article, as of the time of this article download
- Access to high resolution figures
- Links to articles and content related to this article
- Copyright permission to reproduce figures and/or text from this article

View the Full Text HTML

J|A|C|S
ARTICLES
Published on Web 11/13/2007

Fourier Transform Infrared Characterization of a Cu_B−Nitrosyl Complex in Cytochrome *ba*$_3$ from *Thermus thermophilus*: Relevance to NO Reductase Activity in Heme−Copper Terminal Oxidases

Takahiro Hayashi,[‡] I-Jin Lin,[‡] Ying Chen,[†] James A. Fee,[†] and Pierre Moënne-Loccoz*,[‡]

Contribution from Department of Environmental & Biomolecular Systems, OGI School of Science and Engineering, Oregon Health & Science University, 20,000 NW Walker Road, Beaverton, Oregon 97006-8921, and Department of Molecular Biology, The Scripps Research Institute, La Jolla, California 92037

Received June 22, 2007; E-mail: ploccoz@ebs.ogi.edu

Abstract: The two heme−copper terminal oxidases of *Thermus thermophilus* have been shown to catalyze the two-electron reduction of nitric oxide (NO) to nitrous oxide (N_2O) [Giuffre, A.; Stubauer, G.; Sarti, P.; Brunori, M.; Zumft, W. G.; Buse, G.; Soulimane, T. *Proc. Natl. Acad. Sci. U.S.A.* **1999**, *96*, 14718−14723]. While it is well-established that NO binds to the reduced heme a_3 to form a low-spin heme $\{FeNO\}^7$ species, the role Cu_B plays in the binding of the second NO remains unclear. Here we present low-temperature FTIR photolysis experiments carried out on the NO complex formed by addition of NO to fully reduced cytochrome *ba*$_3$. Low-temperature UV−vis, EPR, and RR spectroscopies confirm the binding of NO to the heme a_3 and the efficiency of the photolysis at 30 K. The ν(NO) modes from the light-induced FTIR difference spectra are isolated from other perturbed vibrations using ^{15}NO and $^{15}N^{18}O$. The ν(N−O)a_3 is observed at 1622 cm^{-1}, and upon photolysis, it is replaced by a new ν(N−O) at 1589 cm^{-1} assigned to a Cu_B−nitrosyl complex. This N−O stretching frequency is more than 100 cm^{-1} lower than those reported for Cu−NO models with three N-ligands and for Cu_B^+−NO in bovine *aa*$_3$. Because the UV−vis and RR data do not support a bridging configuration between Cu_B and heme a_3 for the photolyzed NO, we assign the exceptionally low ν(NO) to an O-bound (η^1-O) or a side-on (η^2-NO) Cu_B−nitrosyl complex. From this study, we propose that, after binding of a first NO molecule to the heme a_3 of fully reduced *Tt ba*$_3$, the formation of an N-bound $\{CuNO\}^{11}$ is prevented, and the addition of a second NO produces an O-bond Cu_B−hyponitrite species bridging Cu_B and Fe*a*$_3$. In contrast, bovine cytochrome *c* oxidase is believed to form an N-bound Cu_B−NO species; the [$\{FeNO\}^7\{CuNO\}^{11}$] complex is suggested here to be an inhibitory complex.

Introduction

The reduction of nitric oxide (NO) to nitrous oxide (N_2O) (eq 1) is an obligatory step in the denitrification pathway which converts nitrate and nitrite to dinitrogen gas (N_2).

$$2\,NO + 2\,H^+ + 2\,e^- \rightarrow N_2O + H_2O \qquad (1)$$

Denitrifying NO reductases found in many prokaryotes have been shown to provide these microorganisms resistance to the mammalian immune response. For example, facultative anaerobes such as *Neisseria gonorrhoeae* and *Neisseria meningitidis* depend on NO reductases to tolerate toxic concentrations of NO.[1−3] These integral membrane protein complexes contain a norB subunit evolutionarily related to subunit I of cytochrome *c* oxidase (C*c*O).[4−6] There are no crystal structures for NO reductases yet, but hydropathy plots and sequence alignments show conserved residues involved in the anchoring of cofactors in C*c*O and suggest that strong structural analogies exist in these two families of enzymes. While O_2 reduction in terminal oxidases occurs at a heme−copper dinuclear site, the reduction of NO by NO reductase takes place at a heme/nonheme diiron center.[7−11] Despite the difference in metal composition, some heme−Cu terminal oxidases and heme/nonheme diiron NO reductases are capable of catalyzing the reduction of both NO

[†] Oregon Health & Science University.
[‡] The Scripps Research Institute.

(1) Lissenden, S.; Mohan, S.; Overton, T.; Regan, T.; Crooke, H.; Cardinale, J. A.; Householder, T. C.; Adams, P.; O'Conner, C. D.; Clark, V. L.; Smith, H.; Cole, J. A. *Mol. Microbiol.* **2000**, *37*, 839−855.
(2) Householder, T. C.; Fozo, E. M.; Cardinale, J. A.; Clark, V. L. *Infect. Immun.* **2000**, *68*, 5241−5246.
(3) Anjum, M. F.; Stevanin, T. M.; Read, R. C.; Moir, J. W. *J. Bacteriol.* **2002**, *184*, 2987−2993.
(4) Castresana, J.; Lubben, M.; Saraste, M.; Higgins, D. G. *EMBO J.* **1994**, *13*, 2516−2525.
(5) van der Oost, J.; de Boer, A. P.; de Gier, J. W.; Zumft, W. G.; Stouthamer, A. H.; van Spanning, R. J. *FEMS Microbiol. Lett.* **1994**, *121*, 1−9.
(6) Zumft, W. G.; Braun, C.; Cuypers, H. *Eur. J. Biochem.* **1994**, *219*, 481−490.
(7) Heiss, B.; Frunzke, K.; Zumft, W. G. *J. Bacteriol.* **1989**, *171*, 3288−3297.
(8) Averill, B. A. *Chem. Rev.* **1996**, *96*, 2951−2965.
(9) Wasser, I. M.; de Vries, S.; Moënne-Loccoz, P.; Schroder, I.; Karlin, K. D. *Chem. Rev.* **2002**, *102*, 1201−1234.
(10) Zumft, W. G. *J. Inorg. Biochem.* **2005**, *99*, 194−215.
(11) Moënne-Loccoz, P. *Nat. Prod. Rep.* **2007**, *24*, 610−620.

10.1021/ja074600a CCC: $37.00

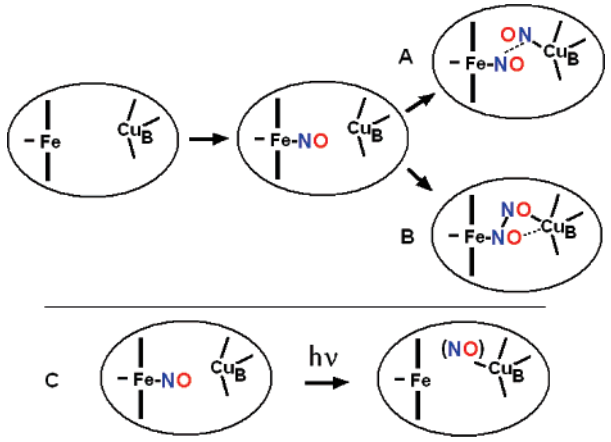

Figure 1. Putative mechanisms of NO reductase in terminal oxidases: [{FeNO}^{7}{CuNO}^{11}] complex (A), Cu_B–O/Fea_3–N bridging hyponitrite complex (B), and the photolysis process in ba_3–NO (C).

and O_2.[12,13] For example, bovine aa_3 oxidase displays no NO-reductase activity while the ba_3 and caa_3 terminal oxidases of *Thermus thermophilus* (*Tt*) do.[13] Because the NO-reductase activity of ba_3 is less than 1% that of denitrifying NO reductases, it is unlikely to be its primary function. However, study of the interaction of NO with ba_3 can expand our knowledge of the chemical behavior of the divergent a_3-Cu_B center as well as help us understand the mechanism of NO reduction at dinuclear sites in general.

The catalytic mechanism of NO reduction in terminal oxidases is generally considered to be initiated by the binding of NO to heme a_3 in the fully reduced enzyme.[13] Subsequent steps are expected to involve Cu_B(I), either as a coordination site for a second NO molecule or as an electron donor and electrostatic partner to a heme a_3–hyponitrite complex (Figure 1).[11,14–16] The initial heme a_3–*nit*rosyl complex is a low-spin Fe(II)–NO, i.e., an $S = 1/2$ {FeNO}^{7} species in Enemark and Feltham notation.[17] Using resonance Raman (RR) spectroscopy, Varotsis and co-workers have shown that the ba_3–NO complex is a six-coordinate species with ν(Fe–NO) and ν(N–O) at 539 and 1620 cm^{-1}, respectively.[14] In addition, Vos and co-workers have monitored the rebinding kinetics of the photolyzed NO, at room temperature in the picosecond to microsecond time scale, and observed no sub-nanosecond NO rebinding to heme a_3.[18] These results strongly support the idea that the photolyzed NO binds transiently to Cu_B before rebinding to heme a_3 in the nanosecond regime. Varotsis and co-workers have attempted to gain information on this photoinduced state at room temperature using time-resolved step-scan FTIR, but the microsecond time resolution of this technique precludes the characterization of a Cu_B–nitrosyl complex.[14] Here we present FTIR photolysis experiments carried out at cryogenic temperatures. Low-temperature UV–vis, EPR, and RR spectroscopies are used to confirm the efficiency of the photolysis, and NO-isotopic labeling permits the isolation of ν(NO) modes from the light-induced FTIR difference spectra. A new ν(N–O) observed at 1589 cm^{-1} is assigned to a Cu_B–nitrosyl complex formed at 30 K. This N–O stretching frequency is more than 100-cm^{-1} lower than those reported for Cu–NO models with three N-ligands and for Cu_B^+–NO in bovine ba_3.[19,20] Our low-temperature UV–vis and RR data do not support a bridging configuration between Cu_B and heme a_3 for the photolyzed NO. Therefore, we conclude that the exceptionally low ν(NO) identifies the Cu_B–nitrosyl complex as either an O-bound (η^1-O) or a side-on (η^2-NO) complex. The relevance of this Cu_B–nitrosyl complex to the NO reductase activity in cytochrome ba_3 is discussed in the context of other terminal oxidases and of denitrifying NO reductases.

Materials and Methods

The expression and purification of ba_3 was performed as previously described.[21] Protein solutions in 20 mM Tris-HCl pH 7.5 with 0.05% dodecyl β-D-maltoside were made anaerobic by prolonged purging with argon on a Schlenk line. Protein solutions were concentrated in a glove box containing less than 1 ppm O_2 (Omnilab System, Vacuum Atmospheres Company) using a microcon filtering device (30 kD cutoff, Biomax, Millipore) to an enzyme concentration of ~350 μM. The sample was fully reduced by addition of 10 mM dithionite in a 1.5-mL tube with a septum top. NO gases (^{14}NO and $^{15}N^{18}O$ purchased from Aldrich, ^{15}NO purchased from ICON) were initially treated with 1 M KOH solution to remove higher nitrogen oxide impurities. NO gas addition to the sample headspace was achieved in the glove box using gastight Hamilton syringes to reach a partial pressure of 0.1 atm of NO. After 1 min of incubation at room temperature, the septum was removed and 18 μL of the protein solution was deposited as a droplet on a CaF_2 window in the anaerobic glove box. A second CaF_2 window was dropped on the sample to form an optical cell with a path length controlled by a 15 μm Teflon spacer. Once the IR cell was securely sealed, the presence of the ba_3–NO complex was confirmed by obtaining the UV–vis spectrum of the sample using a Cary 50 spectrophotometer (Varian). The FTIR cell was then mounted to a closed-cycle cryogenic system (Displex, Advanced Research Systems). Experiments with a 1.0 equiv NO addition were achieved by using diethylamine NONOate as NO donor (Cayman Chemical, Ann Arbor, MI). The NONOate concentration in a 0.01 M NaOH stock solution was determined by UV–vis spectroscopy ($\epsilon_{250} = 9180\ M^{-1}\ cm^{-1}$). The NO produced upon mixing with neutral pH solutions was further confirmed by titration with deoxymyoglobin.

The cryostat was installed in the Cary 50 spectrometer or the sample compartment of the FTIR instrument and kept in the dark while the temperature dropped to 30 K. The temperature of the sample was monitored and controlled with a Cry-Con 32 unit.

FTIR spectra were obtained on a Perkin-Elmer system 2000 equipped with a liquid-N_2-cooled MCT detector and purged with compressed air, dried, and depleted of CO_2 (Purge gas generator, Puregas LLC). Sets of 1000-scan accumulations were acquired at a 4-cm^{-1} resolution. These data-averaging conditions required 15 min, and because of instrumental drift, further accumulation time did not result in an improvement of the FTIR difference spectra. Photolysis of the ba_3–NO complex was achieved with continuous illumination of the samples directly in the FTIR sample chamber with a 50 W tungsten lamp after filtering out heat and NIR emission. The same illumination procedure was used to follow the dissociation-rebinding process by UV–vis spectroscopy with the Cary-50 spectrophotometer.

(12) Fujiwara, T.; Fukumori, Y. *J. Bacteriol.* **1996**, *178*, 1866–1871.
(13) Giuffre, A.; Stubauer, G.; Sarti, P.; Brunori, M.; Zumft, W. G.; Buse, G.; Soulimane, T. *Proc. Natl. Acad. Sci. U.S.A.* **1999**, *96*, 14718–14723.
(14) Pinakoulaki, E.; Ohta, T.; Soulimane, T.; Kitagawa, T.; Varotsis, C. *J. Am. Chem. Soc.* **2005**, *127*, 15161–15167.
(15) Blomberg, M. L.; Blomberg, M. R. A.; Siegbahn, P. E. M. *Biochim. Biophys. Acta* **2006**, *1757*, 31–46.
(16) Ohta, T.; Kitagawa, T.; Varotsis, C. *Inorg. Chem.* **2006**, *45*, 3187–3190.
(17) Enemark, J. H.; Feltham, R. D. *Coord. Chem. Rev.* **1974**, *13*, 339–406.
(18) Pilet, E.; Nitschke, W.; Rappaport, F.; Soulimane, T.; Lambry, J. C.; Liebl, U.; Vos, M. H. *Biochemistry* **2004**, *43*, 14118–14127.
(19) Ruggiero, C. E.; Carrier, S. M.; Antholine, W. E.; Whittaker, J. W.; Cramer, C. J.; Tolman, W. B. *J. Am. Chem. Soc.* **1993**, *115*, 11285–11298.
(20) Zhao, X. J.; Sampath, V.; Caughey, W. S. *Biochem. Biophys. Res. Commun.* **1994**, *204*, 537–543.
(21) Chen, Y.; Hunsicker-Wang, L.; Pacoma, R. L.; Luna, E.; Fee, J. A. *Protein Expression Purif.* **2005**, *40*, 299–318.

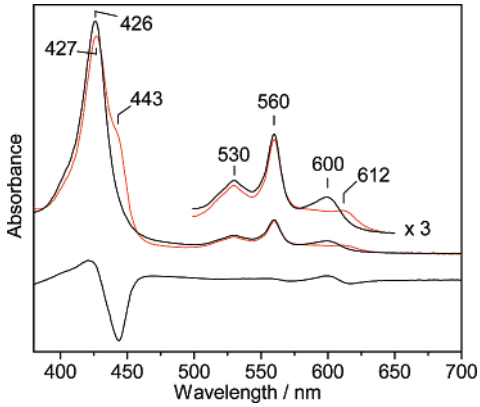

Figure 2. Room-temperature UV−vis spectra of fully reduced cytochrome ba_3 (red) and the ba_3−NO complex (black). The ba_3−NO minus reduced ba_3 difference spectrum is also shown (bottom trace).

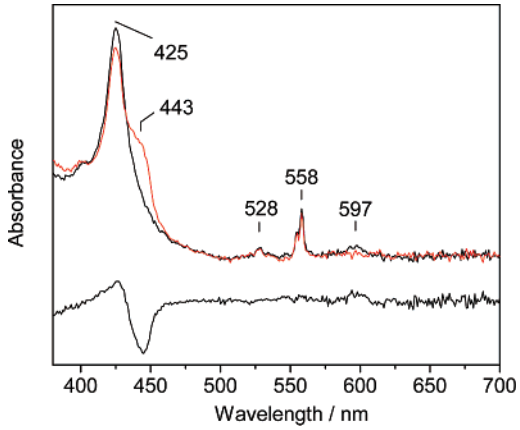

Figure 3. UV−vis spectra of the ba_3−NO complex at 30 K before (black) and after illumination (red). The dark minus illuminated difference spectrum is also shown (bottom trace).

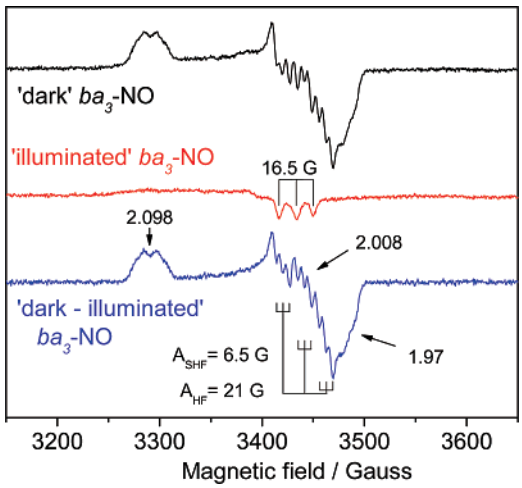

Figure 4. EPR spectra of the ba_3−NO complex at 30 K. Before (black) and after (red) illumination, and the 'dark' minus 'illuminated' difference spectrum (blue). Conditions: protein concentration, 30 μM; temperature, 30 K; microwave frequency, 9.66 GHz; microwave power, 0.2 mW; modulation frequency, 100 kHz; modulation amplitude, 4 G.

The RR samples of reduced ba_3 and ba_3−NO complexes were prepared in a glove box and loaded on a multiwell sample holder mounted to the same closed-cycle cryostat system used in the FTIR experiments. RR spectra were obtained using a backscattering geometry on a custom McPherson 2061/207 spectrograph (set at 0.67 m with variable gratings) equipped with a Princeton Instruments liquid-N_2-cooled CCD detector (LN-1100PB). Kaiser Optical supernotch filters were used to attenuate Rayleigh scattering generated by the 413-nm excitation of an Innova 302 krypton laser (Coherent, Santa Clara CA) and the 442-nm line of a helium−cadmium laser (Liconix, Santa Clara CA). Frequencies were calibrated relative to aspirin, indene, and CCl_4 standards and are accurate to $\pm$ 1 cm^{-1}.

EPR spectra were obtained on a Bruker E500 X-band EPR spectrometer equipped with a superX microwave bridge and a superhigh Q cavity equipped with a nitrogen flow cryostat or a dual mode cavity with a helium flow cryostat (ESR900, Oxford Instruments, Inc.). The experimental conditions, i.e., temperature, microwave power, and modulation amplitude, were varied to optimize the detection of all potential EPR active species. Quantitation of the EPR signals was performed under nonsaturating conditions by double integration and comparison with 0.1 mM and 0.01 mM Cu^{II}(EDTA) standards.

Results

UV−vis and EPR Characterization. Exposure of fully reduced *Tt* ba_3 to an anaerobic headspace containing 0.1 atm NO_g results in the rapid formation of a ba_3−NO complex as indicated by changes in its UV−vis spectrum (Figure 2). Specifically, the Fe(II) heme a_3 Soret band at 443 nm experiences a blue shift to merge with the Fe(II) low-spin heme *b* Soret band at 426 nm. Moreover, the Fe(II) heme a_3 absorption at 612 nm sharpens and shifts to 600 nm upon NO binding. Despite difficulties with background scattering in frozen samples, the same qualitative UV−vis analysis can be performed on FTIR films at cryogenic temperatures (Figure 3).

Prior to illumination, the lack of a 443-nm shoulder in the Soret region and the detection of a well-resolved 597-nm band confirm the presence of the heme a_3−NO complex at 30 K (Figure 3, black trace).[22] However, after a few minutes of illumination with white light, the 443-nm shoulder that is characteristic of the high-spin Fe(II) heme a_3 species is clearly observed at the expense of the 597-nm absorption band from the a_3−NO complex (Figure 3, red trace). While a rigorous quantitative analysis would require the use of glassing agents such as glycerol or ethylene glycol, the low-temperature UV−vis data convincingly show the facile and efficient NO photolysis from heme a_3 to form a photolyzed state which is stable at 30 K. From a comparison of the intensity of the 443-nm shoulder in the UV−vis spectrum of 'illuminated' ba_3−NO and that of 'illuminated' ba_3−CO, we estimate that in the former samples, at least 2/3 of the total heme a_3 content is converted to high-spin after illumination (Figure S1). It is worth pointing out that in these UV−vis spectra obtained at cryogenic temperatures, the α ($Q_{0,0}$) absorption band of the heme *b* is split by $\sim$110 $\pm$ 30 cm^{-1}. Such splitting has been observed previously with several heme *c*- and heme *b*-containing proteins and was assigned to loss of porphyrin symmetry arising from the surrounding protein.[22]

The EPR spectrum of the nonphotolyzed ba_3−NO complex shows a superposition of two signals centered near $g \sim 2$ (Figure 4, top black trace). One signal is readily photolabile and exhibits *g* values (2.098, 2.008, 1.97) and a nine-line ^{14}N-hyperfine structure at g_z (A_{NO} = 21 G, A_{His} = 6.5 G) that are characteristic of six-coordinate heme−nitrosyl with a proximal histidine

(22) Reddy, K. S.; Angiolillo, P. J.; Wright, W. W.; Laberge, M.; Vanderkooi, J. M. *Biochemistry* **1996**, *35*, 12820−12830.

ligand.[23] The second signal is not photolyzed at 30 K, and consequently, the illuminated spectrum shows this isolated signal with its distinctive three-line ^{14}N-hyperfine structure (A_{NO} = 16.5 G) (Figure 4, red trace). Typically, such three-line EPR signals have been assigned to five-coordinate heme−nitrosyl in analogy with low-pH forms of myoglobin−NO and hemoglobin−NO in the presence of allosteric effectors.[24−27] Equivalent three-line EPR signals have been observed in bovine and *P. denitrificans* aa_3−NO and have been assigned alternatively to a five-coordinate a_3−NO subpopulation[28] or to a six-coordinate a_3−NO with distinct orientations of the imidazole and nitrosyl axial ligands[18,29] (vide infra). Significant variations in the relative intensity of these two EPR species were observed among samples, with the three-line EPR species representing as low as 20% in some enzyme preparations but reaching up to 50% in others (Figure S2). On the other hand, using different reducing conditions (10 mM dithionite, and 10 mM ascorbate with 0.1 mM *N*,*N*,*N*′,*N*′-tetramethyl-*p*-phenylenediamine) or different NO concentrations (1 or 5 equiv) had no impact on the relative concentrations of the two heme a_3−NO populations (data not shown). Increasing the protein concentration to 350 μM as used in the FTIR experiments had no effect on the intensity ratio between the two EPR signals (data not shown). While the two heme a_3−NO species are easily distinguished by EPR spectroscopy, the low-temperature UV−vis spectra do not present distinctive features readily assignable to the population with the three-line EPR signal. Similarly, RR experiments fail to detect two distinct heme−nitrosyl complexes (vide infra).

Both EPR and UV−vis experiments show that rebinding of the photolyzed NO to the heme a_3 is inhibited at temperatures below 80 K. This temperature is significantly higher than that measured with the ferrous−nitrosyl complex of myoglobin where rebinding of the photodissociated NO occurs at 40 K.[30] The higher annealing temperature in ba_3−NO suggests that the photolyzed NO is trapped by stabilizing interactions, presumably with Cu_B^+. These results also sharply contrast with that of the ba_3−CO complex where the temperature must be raised above 220 K for CO to dissociate from Cu_B and must, in fact, exit the active site pocket before a new heme a_3−CO complex can form.[31,32] Thus, despite the stabilizing interactions of the photolyzed NO, the data suggest that rebinding of NO to the heme a_3 is facile and does not require its release from the active site pocket. Earlier low-temperature UV−vis and EPR photolysis experiments carried out with bovine C*c*O have reported a similar rebinding temperature dependence.[33,34] As with these early studies, formation of the photolyzed state of ba_3−NO does not result in the appearance of new features in the EPR or UV−vis spectra.

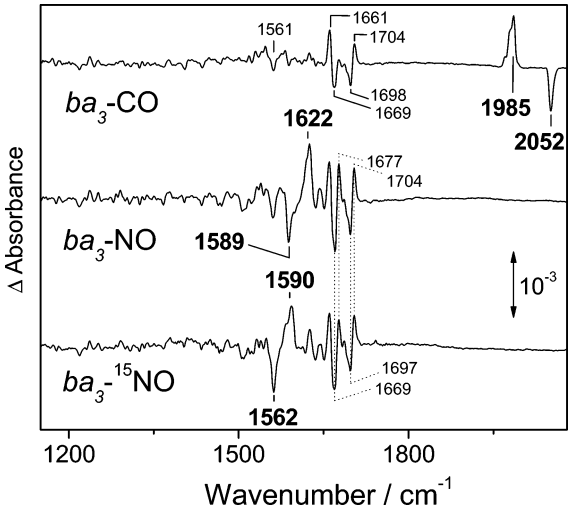

Figure 5. FTIR difference spectra ('dark' minus 'illuminated') of ba_3−CO, ba_3−NO, and ba_3-^{15}NO at 30 K.

FTIR and RR Characterization. Figure 5 shows 'dark' minus 'illuminated' FTIR difference spectra of fully reduced ba_3−NO at 30 K; an FTIR difference spectrum collected on the ba_3−CO complex is also shown for comparison. In the latter complex, ligation of the CO to Cu_B after photolysis from heme a_3 is revealed by the positive ν(C−O)a_3 at 1985 cm^{-1} (i.e., from a_3−CO in the 'dark' spectrum) and the negative ν(C−O)Cu_B at 2052 cm^{-1} (i.e., from the Cu_B−CO in the 'illuminated' spectrum). The ν(CO) vibrations are accompanied by weaker S-shaped signals near and below 1700-cm^{-1} that are insensitive to CO-isotopic labeling (data not shown) and are assigned to the perturbation of amide and porphyrin vibrational modes from the heme a_3.

In the 30 K 'dark' minus 'illuminated' FTIR spectra of ba_3−NO, the positive 1622 cm^{-1} and negative 1589 cm^{-1} features are assigned to ν(N−O) modes on the basis of their −32 and −27 cm^{-1} downshifts with ^{15}N^{16}O, repectively (Figure 5). As with the ba_3−CO complex, a few minutes of white light at 30 K is sufficient to generate these FTIR difference spectra and subsequent illuminations do not produce any further changes. The positive band at 1622 cm^{-1} is attributed to the heme a_3−NO complex based on its photolabile character. This ν(N−O)-a_3 frequency is within a few cm^{-1} of that reported by Varotsis and co-workers.[14] The photoinduced ν(N−O) appears as a negative band at 1589 cm^{-1} and is best extracted from raw data by computing the difference of light-induced difference spectra obtained with different NO-isotopes, i.e., such that modes insensitive to NO-isotopic labeling cancel out (Figure 6). This approach is particularly useful with the ^{15}N^{18}O sample where the superposition of differential signals around 1530 cm^{-1} leads to the apparent lack of a negative ν(^{15}N−^{18}O) (Figure 6, lower red trace). The subtraction of the ^{15}N^{18}O data from those obtained with ^{14}N^{16}O clearly resolves two sets of isotope-sensitive bands. Specifically, the ['dark' minus 'illuminated' ba_3−^{14}N^{16}O] minus ['dark' minus 'illuminated' ba_3−^{15}N^{18}O] spectrum (Figure 6, lower green trace) exhibits a positive band at 1622 cm^{-1} that corresponds to the ν(^{14}N−^{16}O)a_3 and a negative band at 1547 cm^{-1} for ν(^{15}N−^{18}O)a_3. In this same

(23) Yonetani, T.; Yamamoto, H.; Erman, J. E.; Leigh, J. S., Jr.; Reed, G. H. *J. Biol. Chem.* **1972**, *247*, 2447−2455.
(24) Rein, H.; Ristau, O.; Scheler, W. *FEBS Lett.* **1972**, *24*, 24−26.
(25) Wayland, B. B.; Olson, L. W. *J. Am. Chem. Soc.* **1974**, *96*, 6037−6041.
(26) Szabo, A.; Perutz, M. F. *Biochemistry* **1976**, *15*, 4427−4428.
(27) Hille, R.; Olson, J. S.; Palmer, G. *J. Biol. Chem.* **1979**, *254*, 12110−12120.
(28) Pearce, L. L.; Bominaar, E. L.; Hill, B. C.; Peterson, J. *J. Biol. Chem.* **2003**, *278*, 52139−52145.
(29) Pilet, E.; Nitschke, W.; Liebl, U.; Vos, M. H. *Biochim. Biophys. Acta* **2007**, *1767*, 387−392.
(30) Miller, L. M.; Pedraza, A. J.; Chance, M. R. *Biochemistry* **1997**, *36*, 12199−12207.
(31) Dyer, R. B.; Einarsdottir, O.; Killough, P. K.; Lopez-Garriga, J. J.; Woodruff, W. H. *J. Am. Chem. Soc.* **1989**, *111*, 7657−7659.
(32) Einarsdottir, O.; Killough, P. M.; Fee, J. A.; Woodruff, W. H. *J. Biol. Chem.* **1989**, *264*, 2405−2408.
(33) Yoshida, S.; Hori, H.; Orii, Y. *J. Biochem. (Tokyo)* **1980**, *88*, 1623−1627.
(34) Boelens, R.; Rademaker, H.; Pel, R.; Wever, R. *Biochim. Biophys. Acta* **1982**, *679*, 84−94.

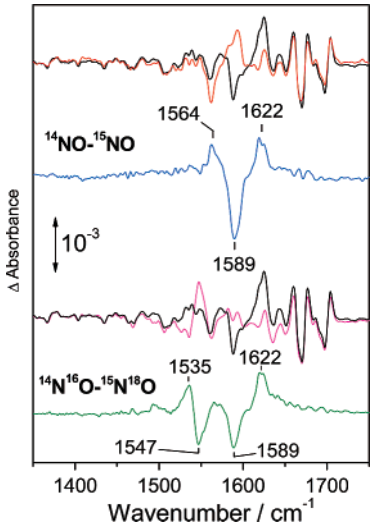

Figure 6. Comparison and difference between 'dark' minus 'illuminated' FTIR difference spectra obtained at 30 K with different NO isotopes in the ba_3−NO complex. Top traces: ba_3−^{14}NO (black), ba_3−^{15}NO (red), and the ba_3−^{14}NO minus ba_3−^{15}NO difference spectra (blue). Bottom traces: ba_3−^{14}N^{16}O (black), ba_3−^{15}N^{18}O (red), and the ba_3−^{14}N^{16}O minus ba_3−^{15}N^{18}O difference spectra (green).

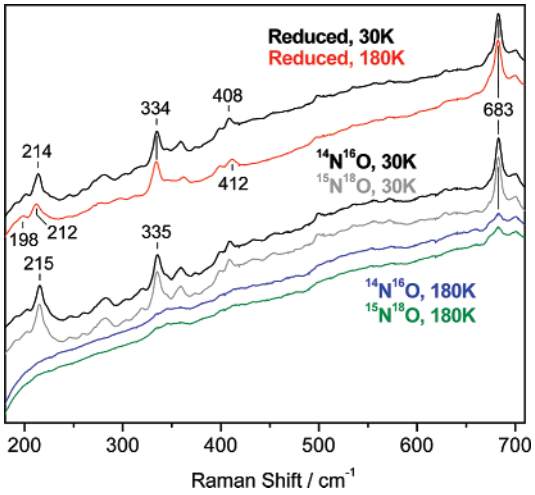

Figure 7. RR spectra obtained with 442-nm excitation at cryogenic temperatures. Top traces: reduced ba_3 at 30 (black) and 180 K (red). Bottom traces: ba_3−NO and ba_3-^{15}N^{18}O at 30 (black and gray) and 180 K (blue and green).

trace, the photoinduced ν(^{14}N−^{16}O) is observed as a negative band at 1589 cm^{-1} and a positive ν(^{15}N−^{18}O) at 1535 cm^{-1}.

The observed frequency and isotopic dependence of the 1589 cm^{-1} signal identifies this mode as an N−O stretching mode of a metal−nitrosyl, and by analogy with the photolysis of the CO complex, we assign this photoinduced signal to an ν(N−O) from a Cu_B−nitrosyl complex. In agreement with the UV−vis and EPR data, the 'dark' FTIR spectrum can be regenerated after annealing the FTIR sample at 90 K, and a new set of 'dark' and 'illuminated' spectra can be collected subsequently. Comparison of successive FTIR difference spectra obtained after annealing above 90 K confirms the reversibility of the photolytic process to produce identical FTIR difference spectra from one cycle to the next (Figure S3). The same is true for successive 'dark' and 'illuminated' UV−vis absorption spectra obtained after annealing at 90 K and returning to 30 K (data not shown) and for these UV−vis experiments being carried out prior or subsequent to the FTIR experiments. These observations demonstrate that the low-intensity white light used in these experiments only induces fully reversible processes involving only the photolysis of the exogenous ligand bound to heme a_3.

Low-temperature RR experiments were carried out to compare the porphyrin vibrational modes of the ferrous heme a_3 in the fully reduced enzyme with those in the photolyzed ba_3−NO complex. A 442-nm excitation provides selective enhancement of the ferrous heme a_3 vibrations, and the fully reduced ba_3 exhibits two low-frequency modes at 193 and 209 cm^{-1} that have been assigned to heme a_3 iron(II)−histidine stretches on the basis of their downshift with ^{57}Fe.[35,36] While these two bands are of comparable intensity at 10 °C,[35] the ν(Fea_3−His) at 214 cm^{-1} becomes the major component at 30 K (Figure 7, top black trace).[37] When the same experimental conditions are used with ba_3−^{14}N^{16}O and ba_3−^{15}N^{18}O samples at 30 K (Figure 7, bottom black and gray traces), the 442-nm laser line provides an effective means of fully dissociating the heme a_3−nitrosyl complex, and an intense RR band at 215 cm^{-1} is assigned to the ν(Fea_3−His) in the photolyzed ba_3−NO complex. The 1-cm^{-1} upshift of the ν(Fea_3−His) in the photodissociated state relative to the resting state of the fully reduced enzyme[38] is reminiscent of the 6- to 8-cm^{-1} upshift observed in time-resolved RR experiments with the CO complex of bovine C*c*O and suggests that the heme a_3 is trapped in a nonequilibrium conformation.[39,40] The detection of this ν(Fea_3−His) mode confirms that, following the photolysis of NO from heme a_3, Fea_3^{2+} is in a five-coordinate high-spin state equivalent to that of the fully reduced resting enzyme and thus is not involved in a bridging coordination of the photolyzed NO with Cu_B^+.

The RR spectra of the ba_3−NO samples obtained at 180 K, where rapid rebinding of photolyzed NO to the heme a_3 occurs and prevents trapping of the photolyzed state, are also shown in Figure 7 (bottom blue and green traces). Because ν(Fe−His) modes are resonance enhanced only in five-coordinate high-spin Fe(II) heme species,[41] no ν(Fea_3−His) is detected in the ba_3−NO samples at 180 K, and the 442-nm excitation provides only weak preresonance Raman conditions for both heme a_3−NO and low-spin heme *b*. In contrast, the fully reduced enzyme continues to display ν(Fe−His) modes similar to those observed at 30 K (Figure 7). RR experiments with 413-nm excitation at 180 K also confirm the presence of heme a_3−NO complexes (Figure S4). Specifically, the heme a_3−NO complex displays ν_4, ν_3, ν_2, and ν_{10} at 1370, 1496, 1595, and 1632 cm^{-1}, respectively, and a ν(Fe−NO) at 544 cm^{-1} that shifts by −17 cm^{-1} with ^{15}N^{18}O. As with the low-temperature UV−vis data,

(35) Oertling, W. A.; Surerus, K. K.; Einarsdottir, O.; Fee, J. A.; Dyer, R. B.; Woodruff, W. H. *Biochemistry* **1994**, *33*, 3128−3141.
(36) Gerscher, S.; Hildebrandt, P.; Buse, G.; Soulimane, T. *Biospectroscopy* **1999**, *5*, S53−63.
(37) Because our Raman measurements utilize notch filters to attenuate the Raleigh scattering and can produce baseline perturbations below 200 cm^{-1}, minor changes in this region are not discussed.
(38) While our instrumentation measures absolute Raman frequencies within 1 cm^{-1}, relative shifts of <0.6 cm^{-1} can be reliably measured when two spectra are collected successively with no modification of the optical alignment and the spectrograph settings.
(39) Findsen, E. W.; Centeno, J.; Babcock, G. T.; Ondrias, M. R. *J. Am. Chem. Soc.* **1987**, *109*, 5367−5372.
(40) Lou, B. S.; Larsen, R. W.; Chan, S. I.; Ondrias, M. R. *J. Am. Chem. Soc.* **1993**, *115*, 403−407.
(41) Kitagawa, T., Heme protein structure and the iron-histidine stretching mode. In *Biological applications of Raman spectroscopy. Vol. 3. Resonance Raman spectra of hemes and metalloproteins*; Spiro, T. G., Ed.; John Wiley & Sons: New York, 1988; Vol. 3, pp 97−131.

and in contrast with the EPR data, the low-temperature RR spectra provide no support for the presence of a significant five-coordinate heme−nitrosyl population. Indeed, five-coordinate heme {FeNO}^{7} species display porphyrin modes that are upshifted ∼5 cm^{-1} from their six-coordinate counterparts. Their ν(Fe−NO) and ν(N−O) modes are also affected by the absence of a sixth trans ligand and are observed ∼−20 cm^{-1} and ∼+50 cm^{-1}, respectively, from their six-coordinate counterparts.

Discussion

Five-coordinate ferrous heme irons exhibit high affinities for NO, and formation of heme a_3−nitrosyl complexes in fully reduced heme−copper terminal oxidases is demonstrated by UV−vis, EPR, and vibrational spectroscopies.[14,20,42−47] In bovine C*c*O, at high NO concentration, evidence for the binding of a second NO molecule to Cu_B^+ is based on the disappearance of the a_3−NO EPR signal and the detection of two ν(NO)s in the FTIR spectra: one at 1610 cm^{-1} assigned to a_3−NO, and one at 1700 cm^{-1} assigned to Cu_B^+−NO.[20,44] Only a few Cu−nitrosyl complexes have been fully characterized so far, but N_3−Cu−NO model compounds synthesized by Tolman and co-workers have ν(N−O)s between 1712 and 1753 cm^{-1}, in good agreement with the data on bovine C*c*O−NO.[19,48] Presumably, the lack of NO reductase activity in bovine C*c*O allows for the accumulation of a stable [{FeNO}^{7}/{CuNO}^{11}] complex. In contrast, binding of a second NO molecule in ba_3−NO is proposed to result in the formation of a N−N bond and the eventual release of N_2O.[14] Whether Cu_B^+ in ba_3 binds NO, even transiently, remains unclear since the attack of a_3−NO by a second NO molecule may occur without its coordination to Cu_B^+ (Figure 1).[15] Flash photolysis experiments on the ba_3−NO complex carried out at room-temperature reveal efficient geminate rebinding of NO to the heme a_3 with a time constant of 15 ns.[18] This rapid rebinding rate precludes characterization of the photolyzed state of ba_3 using step-scan FTIR spectroscopy since the time resolution of this technique is limited to the μs range.[14]

Using cryogenic temperatures, we were able to trap the photolysis product of ba_3−NO and identify a novel ν(NO) at 1589 cm^{-1}. The complete and facile formation of this photolyzed state by illumination of the ba_3−NO complex with a diffuse 50-W white light limits the realm of this photoprocess to the dissociation of the exogenous ligand from heme a_3, as previously observed with ba_3−CO. Low-temperature UV−vis and RR spectra suggest that the heme a_3 does not interact with the photolyzed NO group in any significant manner, and thus, by analogy with the photolysis process in ba_3−CO, the novel ν(NO) at 1589 cm^{-1} is assigned to a Cu_B−nitrosyl complex. However, this ν(NO) frequency is exceptionally low and contrasts with terminally bound M−NO complexes, which typically display ν(NO)s above 1650 cm^{-1}.[49] A bridging coordination of the photolyzed NO group between heme a_3 and Cu_B may explain the observed ν(NO) since multinuclear inorganic complexes with bridging nitrosyl groups adopt μ-1,1 N-bound bridging geometries with ν(NO)s near 1500 cm^{-1}.[49] This interpretation however, is not supported by the UV−vis and RR features of the heme a_3 in the photolyzed ba_3−NO complex which are practically indistinguishable from those of the histidine-bound five-coordinate heme a_3^{2+}. Thus, we favor an assignment of the 1589-cm^{-1} ν(NO) to an NO bound to Cu_B^+ either in an O-bound or side-on geometry. Precedent for such NO coordination to transition metals is beginning to accumulate.[50,51] Light-induced isomerization of {OsNO}^{6}, {RuNO}^{6}, {FeNO}^{6}, and {FeNO}^{7} complexes to O-bound and/or side-on conformers are associated with large downshifts in ν(NO).[52−54] In the case of porphyrin {FeNO}^{7} models, N-bound isomers, with ν(NO)s near 1670 cm^{-1}, experience downshifts of ∼140 cm^{-1} upon light-induced isomerization.[54] Synthetic models of O-bound isomers of {CuNO}^{11} species have yet to be reported, but this is hardly surprising in view of the scarcity of characterized {CuNO}^{11} species as a whole. While the investigation of Cu−nitrosyl complexes in metalloproteins is equally scarce, the type-II copper of nitrite reductase has been shown, crystallographically, to coordinate NO with a side-on geometry.[55,56] Recent DFT calculations comparing the energetics of end-on and side-on {CuNO}^{11} species with type 2 copper sites also support the relevance of side-on isomers.[57] Moreover, the model predicts a 0.05-Å lengthening of the N−O bond in the side-on isomer compared to the end-on isomer which would result in a downshift of the ν(N−O) frequency. Thus, we interpret our FTIR spectra as direct evidence for the formation of a side-on Cu_B−nitrosyl complex in *Tt* ba_3.

The low ν(NO) in the photolysis product of ba_3−NO suggests a {CuNO}^{11} species that should be viewed as a Cu_B^{2+}−NO$^-$ rather than a Cu_B^+−NO species. The latter formulation implies a cuprous d^{10} electronic configuration with an $S = 1/2$ NO ligand and is expected to produce an overall $S = 1/2$ species with an EPR signal centered around $g \sim 2$. In contrast, a Cu_B^{2+}−NO$^-$ formulation suggests an $S = 1/2$ cupric center coupled to an $S = 1$ NO$^-$ ligand to produce an $S = 3/2$ or $S = 1/2$ species depending on whether ferromagnetic or antiferromagnetic coupling occurs. The latter description of the {CuNO}^{11} species is equivalent to that of a nonheme {FeNO}^{7} species, which is described as an $S = 3/2$ species with an $S = 5/2$ high-spin ferric center antiferromagnetically coupled to an $S = 1$ NO$^-$ ligand.[58] On the basis of this analogy, an EPR signal at $g \sim 4$ or $g \sim 2$ would be expected for the Cu_B−nitrosyl complex in ba_3;

(42) Blokzijl-Homan, M. F.; van Gelder, B. F. *Biochim. Biophys. Acta* **1971**, *234*, 493−498.
(43) Stevens, T. H.; Brudvig, G. W.; Bocian, D. F.; Chan, S. I. *Proc. Natl. Acad. Sci. U.S.A.* **1979**, *76*, 3320−3324.
(44) Brudvig, G. W.; Stevens, T. H.; Chan, S. I. *Biochemistry* **1980**, *19*, 5275−5285.
(45) Mascarenhas, R.; Wei, Y. H.; Scholes, C. P.; King, T. E. *J. Biol. Chem.* **1983**, *258*, 5348−5351.
(46) Blackmore, R. S.; Greenwood, C.; Gibson, Q. H. *J. Biol. Chem.* **1991**, *266*, 19245−19249.
(47) Vos, M. H.; Lipowski, G.; Lambry, J. C.; Martin, J. L.; Liebl, U. *Biochemistry* **2001**, *40*, 7806−7811.
(48) Schneider, J. L.; Carrier, S. M.; Ruggiero, C. E.; Young, V. G., Jr.; Tolman, W. B. *J. Am. Chem. Soc.* **1998**, *120*, 11408−11418.
(49) Nakamoto, K. *Infrared and Raman spectroscopy of inorganic and coordination compounds*, 5th ed.; John Wiley and Sons, Inc.: New York, 1997; Vols. A, B.
(50) Coppens, P.; Novozhilova, I.; Kovalevsky, A. *Chem. Rev.* **2002**, *102*, 861−883.
(51) Novozhilova, I. V.; Coppens, P.; Lee, J.; Richter-Addo, G. B.; Bagley, K. A. *J. Am. Chem. Soc.* **2006**, *128*, 2093−2104.
(52) Fomitchev, D. V.; Coppens, P. *Inorg. Chem.* **1996**, *35*, 7021−7026.
(53) Fomitchev, D. V.; Coppens, P.; Li, T. S.; Bagley, K. A.; Chen, L.; Richter-Addo, G. B. *J. Chem. Soc., Chem. Commun.* **1999**, 2013−2014.
(54) Cheng, L.; Novozhilova, I.; Kim, C.; Kovalevsky, A.; Bagley, K. A.; Coppens, P.; Richter-Addo, G. B. *J. Am. Chem. Soc.* **2000**, *122*, 7142−7143.
(55) Tocheva, E. I.; Rosell, F. I.; Mauk, A. G.; Murphy, M. E. P. *Science* **2004**, *304*, 867−870.
(56) Antonyuk, S. V.; Strange, R. W.; Sawers, G.; Eady, R. R.; Hasnain, S. S. *Proc. Natl. Acad. Sci. U.S.A.* **2005**, *102*, 12041−12046.
(57) Wasbotten, I. H.; Ghosh, A. *J. Am. Chem. Soc.* **2005**, *127*, 15384−15385.
(58) Brown, C. A.; Pavlosky, M. A.; Westre, T. E.; Zhang, Y.; Hedman, B.; Hodgson, K. O.; Solomon, E. I. *J. Am. Chem. Soc.* **1995**, *117*, 715−732.

however, despite our efforts, we were not able to detect an EPR signal associated with the photolyzed state of the enzyme. The lack of an EPR signal may originate from a rapid intramolecular electron transfer between Cu^+ and $NO^\bullet$ that results in signal broadening beyond detection. Magnetic coupling of the $\{CuNO\}^{11}$ species with the $S = 2$ high-spin ferrous heme a_3 may also render the heme−Cu dinuclear center EPR silent. Finally, environmental effects could also play an important role in the EPR-silent character of some $\{CuNO\}^{11}$ species since Tolman and co-workers have noted that the addition of π-electron systems in Cu−NO model complexes can result in the disappearance of EPR activity.[48]

Our EPR data obtained prior to photolysis also deserve further discussion. The nine-line and three-line $g \sim 2$ signals observed in our experiments with ba_3−NO are similar to those reported earlier for heme a_3−NO complexes in other terminal oxidases,[18,28] but the presence of these two populations in ba_3−NO is in apparent conflict with earlier reports by Pilet and coworkers.[18,29] Indeed, while Pilet et al. observed both the nine-line and three-line EPR features in *P. denitrificans* aa_3−NO, they observed no three-line signal in their EPR spectra of ba_3−NO.[18] In *P. denitrificans* aa_3−NO, the appearance of the three-line $g \sim 2$ signal was dependent on the number of NO equiv added and was accompanied by a second signal at $g \sim 4$ assigned to an $S = 3/2$ Cu_B−NO complex.[18] These same authors have proposed that binding of a second NO molecule at the heme−Cu site results in a reorientation of the heme a_3 proximal histidine plane perpendicular to, rather than parallel to, the plane of the Fe−N−O unit.[18] However, the structural event that leads to the heme a_3−NO three-line EPR signal in *Tt* ba_3 must be different since our measurements show that the three-line $g \sim 2$ signal is observed without the accompanying $g \sim 4$ signal and without a clear dependence on the NO concentration. Additional experiments are underway with *Tt* ba_3 and other heme−copper terminal oxidases in an effort to better establish the origin of these EPR signals.

Several structural characteristics may determine the proficiency of a given terminal oxidase with regard to NO reductase activity, and proposing distinct isomer forms of Cu_B−nitrosyl complexes in terminal oxidases has mechanistic significance. For example, the distance between the two metal ions at the active site is likely to be important for NO reductase activity. In *P. denitrificans* cNOR, the iron−iron distance is ≤3.5 Å and could favor the formation of an N−N bond between two metal−nitrosyl complexes.[11,59] Crystal structures of terminal oxidases have revealed a range of Fea_3−Cu_B distances. In oxidized *Tt* ba_3, the heme−copper distance is 4.4 Å[60,61] while in bovine C*c*O, it varies between 4.9 and 5.3 Å depending on the state of the enzyme.[62] Similarly, in *P. denitrifcans* aa_3, the Fea_3−Cu_B distance varies between 4.5 and 5.2 Å depending on the presence of an auxiliary subunit complementing the subunit I/subunit II core complex.[63,64] Also noteworthy is the observation that heme−copper terminal oxidases form both five- and six-coordinate heme $\{FeNO\}^7$ species.[14,18,28,65] Undoubtedly, the coordination number must impact the fate of the NO reaction at the dinuclear active site.

Our current data suggest that the manner in which Cu_B^+ interacts with NO may also determine whether or not NO reductase activity will be observed. Specifically, while a heme/nonheme $[\{FeNO\}^7]_2$ complex in cNOR is believed to be catalytically competent,[11,66] the formation of an N-bound Cu_B−NO complex in bovine aa_3 may lead to an inhibitory $[\{FeNO\}^7$-$\{CuNO\}^{11}]$ dead-end complex (Figure 1A), in part at least because of the greater metal−metal distance in bovine aa_3 compared to cNOR. Instead, the NO reductase activity in *Tt* ba_3 may be based on the formation of a $\{CuON\}^{11}$ species or the concerted formation of Cu_B−O and N−N bonds between a free NO molecule and the heme a_3−nitrosyl complex to form a bridging hyponitrite between Cu_B and Fea_3 (Figure 1B). Comparative cryogenic FTIR photolysis studies with other terminal oxidases and denitrifying NO reductases are underway.

Acknowledgment. This work was supported by the National Institutes of Health (P.M.-L., GM 074785; J.A.F., GM 35342). We thank Dr. James Whittaker for the use of his liquid helium cryostat for the EPR experiments.

Supporting Information Available: Low-temperature UV−vis spectra of ba_3−CO and ba_3−NO before and after illumination, EPR spectra of ba_3−NO samples generated from different protein purification batches, successive FTIR difference spectra of ba_3−NO obtained after an annealing cycle, and low-temperature RR spectra obtained with 413-nm excitation. This material is available free of charge via Internet at http://pubs.acs.org.

JA074600A

(59) Moënne-Loccoz, P.; Richter, O.-M. H.; Huang, H. W.; Wasser, I. M.; Ghiladi, R. A.; Karlin, K. D.; de Vries, S. *J. Am. Chem. Soc.* **2000**, *122*, 9344−9345.
(60) Soulimane, T.; Buse, G.; Bourenkov, G. P.; Bartunik, H. D.; Huber, R.; Than, M. E. *EMBO J.* **2000**, *19*, 1766−1776.
(61) Hunsicker-Wang, L. M.; Pacoma, R. L.; Chen, Y.; Fee, J. A.; Stout, C. D. *Acta Crystallogr.* **2005**, *D61*, 340−343.
(62) Yoshikawa, S.; Shinzawa-Itoh, K.; Nakashima, R.; Yaono, R.; Yamashita, E.; Inoue, N.; Yao, M.; Fei, M. J.; Libeu, C. P.; Mizushima, T.; Yamaguchi, H.; Tomizaki, T.; Tsukihara, T. *Science* **1998**, *280*, 1723−1729.
(63) Iwata, S.; Ostermeier, C.; Ludwig, B.; Michel, H. *Nature* **1995**, *376*, 660−669.
(64) Ostermeier, C.; Harrenga, A.; Ermler, U.; Michel, H. *Proc. Natl. Acad. Sci. U.S.A.* **1997**, *94*, 10547−10553.
(65) Pinakoulaki, E.; Stavrakis, S.; Urbani, A.; Varotsis, C. *J. Am. Chem. Soc.* **2002**, *124*, 9378−9379.
(66) Kumita, H.; Matsuura, K.; Hino, T.; Takahashi, S.; Hori, H.; Fukumori, Y.; Morishima, I.; Shiro, Y. *J. Biol. Chem.* **2004**, *279*, 55247−55254.